This paper is published as part of a *CrystEngComm* themed issue on:

Biomineralisation

Guest edited by Lia Addadi
The Weizmann Institute of Science, Israel

Published in issue 12, 2007 of *CrystEngComm*

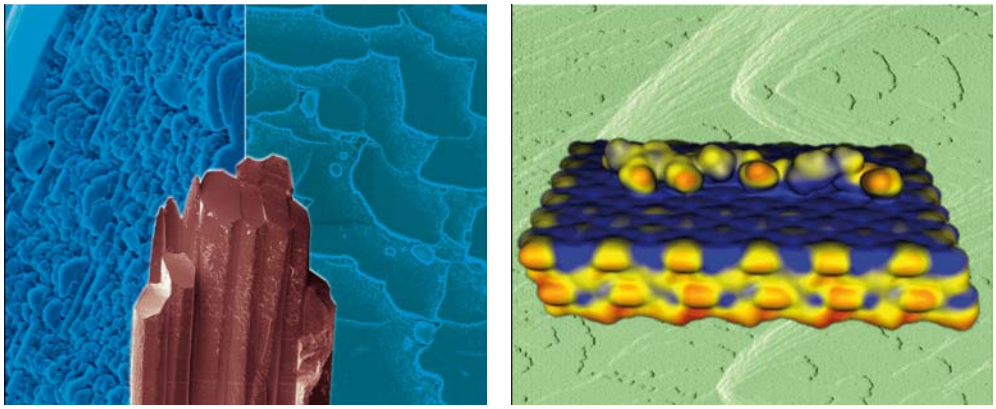

Images reproduced by permission of Lia Addadi (outside) and James De Yoreo (inside)

Other papers published in this issue include:

Molecular dynamics simulations of the interaction of citric acid with the hydroxyapatite (0001) and (01-10) surfaces in an aqueous environment
N. H. de Leeuw and J. A. L. Rabone, *CrystEngComm*, 2007, **DOI:** 10.1039/b710974a

Synthesis-dependant structural variations in amorphous calcium carbonate
Raymond S. K. Lam, John M. Charnock, Alistair Lennie and Fiona C. Meldrum, *CrystEngComm*, 2007, **DOI:** 10.1039/b710895h

Calcite shape modulation through the lattice mismatch between the self-assembled monolayer template and the nucleated crystal face
Boaz Pokroy and Joanna Aizenberg, *CrystEngComm*, 2007, **DOI:** 10.1039/b710294a

Fine structure of nacre revealed by solid state ^{13}C and ^{1}H NMR
Christian Jäger and Helmut Cölfen, *CrystEngComm*, 2007, **DOI:** 10.1039/b708600h

Visit the *CrystEngComm* website for cutting-edge crystal engineering research

www.rsc.org/crystengcomm

Structural adaptability in an organic template for $CaCO_3$ mineralization

Elaine DiMasi,*[a] Seo-Young Kwak,†[a] Benoît P. Pichon‡[b] and Nico A. J. M. Sommerdijk*[bc]

Received 20th July 2007, Accepted 10th October 2007
First published as an Advance Article on the web 24th October 2007
DOI: 10.1039/b711153c

Biomimetic strategies to control mineral nucleation include the development of self-assembled monolayers with appropriate structural properties. We present a bis-urea based surfactant with variable structural adaptability, which induces habit modification in calcite crystals under optimal conditions. *In situ* surface-sensitive synchrotron X-ray scattering measurements are reported, which yield surprising conclusions for the film structure. In particular, it is found that nucleation of modified calcite is correlated with the release of two-dimensional ordering in the surfactant layer. The model system is discussed in the context of the history of Langmuir films as models for biomineralization.

Introduction

Biological minerals inspire unique approaches to crystal engineering. In biominerals, organic species are understood to play several roles to control mineralization. Organic macromolecules and assemblies affect local concentrations of ions, provide physical confinement, and in many cases have distinct tertiary structures of their own with provocative relationships to the structure, orientation, or shape of adjacent mineral crystals. In the wake of such observations, which have been reviewed many times, an enormous amount of recent effort has gone into biomimetic crystal engineering through use of synthetic templates designed to control mineralization. A template by definition interacts with mineral surfaces directly. Recognition between organic molecules and mineral particles may arise from a close structural match, or from favorable chemical interactions between functional groups and mineral ions, nuclei, or precursor particles.

Within this toolbox for organic templating of minerals, one tool—adaptability of the template—remains underutilized. This is surprising since the typical macromolecule has many more structural degrees of freedom than a stable crystalline mineral, and cannot be expected to remain rigid during mineralization. The organic structure should presumably be just malleable enough to optimize the desired interactions. A template too flexible will not control mineralization (not in the sense of a template). The opposite extreme, a rigid organic template which can force nucleation of preferred crystal faces by an epitaxial process as solid state systems can, no matter what the environmental conditions, has not yet been proven to exist. Of course, detecting structural changes in the organic assembly while the mineral forms is only possible in a model system designed to facilitate the appropriate *in situ* measurements. The structural changes could be expected to be very subtle.

Langmuir monolayers assembled on aqueous subphases are, in this context, perfect model systems for the study of template–mineral interactions. *In situ* surface-sensitive synchrotron X-ray scattering techniques make it possible to measure the two-dimensional lattice parameters of Langmuir films with high precision, and to detect molecular tilts, film thickness profiles, and other structural details. At the same time, the experiments are perfectly sensitive to formation of minerals at the surface, and can reliably measure crystal phase and orientation. In fact, the development of the scattering techniques parallels the development of biomimetic Langmuir monolayer mineralization experiments, two streams of research which converged definitively just a few years ago.

Our aim in the present article is twofold. By way of introduction, we will review points of interest in the dual timelines of Langmuir monolayer research with respect to mineralization and to *in situ* X-ray scattering, and outline the intermittent attention paid to template adaptability. We will highlight one system which is indeed known to exemplify a structural match between an organic film and a mineral nucleated beneath it. Notably, the organic template and the mineral adapt to each other, with the lattice constants of both phases modified relative to those found for each separately. This sets the stage for our main interest in this paper, which is to present a recently developed family of surfactant molecules which were designed to have varying degrees of adaptability. The surfactants nucleate calcium carbonate with preferential orientations, according to their degree of structural adaptability. While previous publications have given the details of characterization and mineralization experiments, here we tell the story of interpretation of the X-ray scattering results in detail. A notable theme of the investigation has been that a truly adaptable template takes the necessary shape for the job it has to accomplish, which is not necessarily the same as the structure its designers may have intended for it!

[a]*National Synchrotron Light Source, Brookhaven National Laboratory, Upton NY 11973, USA. E-mail: dimasi@bnl.gov*
[b]*Laboratory for Molecular and Organic Chemistry, Eindhoven University of Technology, P.O.Box 513, 5600 MB Eindhoven, The Netherlands. E-mail: N.Sommerdijk@tue.nl*
[c]*Soft Matter CryoTEM Research Unit, Eindhoven University of Technology, P.O.Box 513, 5600 MB Eindhoven, The Netherlands*
† Present address: Department of Biomineralization, The Forsyth Institute, Boston MA 02115, USA.
‡ Present address: Institut de Physique et de Chimie des Materiaux, 23 rue du Loess, BP43, 67034 Strasbourg, Cedex 2, France.

Langmuir films as templates

Templating as we understand it here requires two elements: the *transfer of structural information* from the template to the nucleating phase, and *demonstrable interactions* between the organic and inorganic. The stage was set to establish both of these over 25 years ago in Langmuir films assembled at air–water interfaces. Langmuir monolayer (LM) systems are chemically and structurally tunable, they allow control over the chemistry of the subphase and, most important for structural studies and molecular modeling, they can be truly flat at the molecular level, over mm scales along their surfaces. This latter idealization is untrue for self-assembled films on solids and for biological organic matrices. Hence, film–solute interactions have been under study in LM systems for many years. A 1982 paper demonstrated the interactions of heavy metal cations with stearic acid monolayers, based on effects measured in pressure–area isotherms.[1] In 1985, homochiral LMs of amphiphilic α-amino acid molecules were prepared and demonstrated to selectively nucleate crystals of glycine from the subphase solution.[2] The observation of enantiomorphous pyramidal glycine crystals with basal (010) or $(0\bar{1}0)$ faces depending on film chirality confirmed the transfer of structure from film to nucleated crystal. Nucleation of calcite on polymer surfaces functionalized with aspartate, in imitation of biomineralizing organic matrices, was reported in 1987.[3] Meanwhile, the determination of molecular structure in LMs by diffraction was also under development: synchrotron X-ray and neutron facilities had just made it possible to make scattering measurements in reflection and grazing-incidence geometries from the water surface *in situ*.[4]

It was in the context of this body of knowledge that Mann, Heywood, Rajam, and Birchall announced the controlled crystallization of $CaCO_3$ under stearic acid monolayers.[5] It is worth reiterating why this paper is so influential. First: it explicitly linked the monolayer studies to *biomineralization*, a new context for both fields. Second: it proposed that the initial stage of mineral nucleation by the film is the establishment of the Stern layer of bound cations, an experimentally accessible hypothesis. Third: it brought the idea of epitaxial lattice matching into the discussion (from an origin in other biomineral literature, where ordered organic matrices had been discussed) *and*, fourth, declared that the observed results actually did not involve epitaxial lattice matching. Instead (fifth), stereochemical and electrostatic matching were predominant and could override the structural mismatch. A sixth contribution of the work is its note that partially-compressed films were optimal in controlling vaterite crystal orientation and size, perhaps because this requires the Ca-induced local ordering of stearate molecules into a configuration tailored for nucleation. This statement is a prelude to the mechanism of *template adaptability* which motivates the present work.

Mineralization at monolayer films

This 1988 paper stimulated a burst of activity in mineralizing monolayer films of all kinds, which have been repeatedly but somewhat selectively reviewed. Longer stories about $CaCO_3$–stearate were published by the same group, detailing exactly when calcite *versus* vaterite could be formed and exploring the mechanisms mentioned above.[6] When the $CaCO_3$ mineralization work was extended to LMs of docosanoate, octadecylamine, octadecanol, and cholesterol, headgroup charge was the primary variable: negatively charged fatty acids produced macroscopically oriented crystals.[7–9] At the same time, these papers state that the same films, mineralized with different types of mineral solutions or at different rates, led to different crystallization results—calling into question the predominance of the molecular recognition described previously. The group studied $BaSO_4$ nucleation under films with sulfonate, phosphonate, and carboxylate headgroups; calling the epitaxial process a central tenet of biomineralization, the authors concluded from their data that since sulfonate and phosphonate headgroups nucleated a preferred (100) face (despite poor lattice matching) while the carboxylate did not, stereochemical effects are of overriding importance.[10–12] The capacity for highly ordered organic interfaces to catalyze inorganic crystallization was also emphasized. By contrast, nucleation of hydrated phase gypsum ($CaSO_4 \cdot H_2O$) under charged *versus* polar surfactants led to the conclusion that charge and stereochemical interactions were not selective in that case, but that hydrogen bonding at the crystal–monolayer interface was.[13] Aragonite, another $CaCO_3$ polymorph, was eventually added to the list of oriented crystals observed, being nucleated under different LMs with the help of $MgCl_2$ added to the calcium bicarbonate subphase; again, detailed discussion of atomic relationships in the film and crystal planes was given.[14] Heywood and Mann reviewed their work in 1994, again emphasizing the cooperative influences of film charge and stereochemical disposition.[15]

At the same time, another group presented *kinetic* data for an LM-templated system, ice under alcohol monolayers.[16] These experiments were based on observing induction times for ice nucleation with and without the monolayer, and the authors concluded that the monolayer affected neither the free energy for forming a critical nucleus, nor the critical nucleus size; but they argued that the structural match between the hydroxyl array and the basal plane of hexagonal ice was necessary to catalyze the heterogeneous ice nucleation. The study of molecular recognition *versus* other factors continued now among many research groups: calcium phosphate at stearic acid LMs (lattice mismatch 22%);[17] CdS under arachidic acid (lattice mismatch 1–4%);[18] PbS under arachidic acid–octadecylene mixtures (square lattice parameter of cations "matching" $\sqrt{3}/2 \times$ triangular lattice parameter of surfactant);[19] CdS and ZnS under octadecanoyl mercaptan(3) (no orientation to monolayer reported);[20] Cu and Na sulfate minerals under diazafluorenone amphiphile (selecting (010) faces compatible with the model monolayer structure)[21,22] and other films;[23–25] calcite under porphyrin amphiphiles (nucleating plane (00.1) consistent with model monolayer structure);[26] oriented KH_2PO_4 beneath lipid monolayers.[27,28] Epitaxial (3% mismatch) (010) γ-FeO(OH) under stearyl alcohol layers converted by dissolution–precipitation into a nonoriented Fe_3O_4 particulate film.[29] Fe complexes were induced by photoirradiation (no structural relationship to monolayer reported).[30]

Indeed, a review of mineralization under LMs from the present remove shows just how much variability exists in

mineral templating. Calvert and Rieke reviewed this literature in 1996 and emphasized the high degree of structural flexibility inherent in organic surfaces. They pointed out cases where an apparent lack of influence of monolayer compression suggests that the monolayer adapts the necessary conformation at the site of nucleation.[31] Cooper, Sessions, and Lubetkin studied amino acid nucleation under partially compressed films and concluded that the ability of the film to reorganize to reduce interfacial energy can optimize nucleation.[32,33] In subsequent publications a mixture of mechanisms began to be represented, with some still emphasizing structure-based molecular recognition[34–38] and others discussing interfacial electrostatics as the predominant mechanism.[39–49] Experiments which highlighted the importance of monolayer adaptability included calcium oxalate grown under phospholipid films;[50–52] hydroxyapatite under fatty acids;[53] observations by Brewster Angle Microscopy of mineralization at domain boundaries of Langmuir films, where it can be argued that molecules shift to accommodate crystal nuclei;[54,55] and computational studies.[56]

In situ X-ray scattering literature

A notable frustration in this literature was the lack of direct structural information from *in situ* diffraction. It turns out that in 1988, the same year in which that first $CaCO_3$–stearate paper was published, an X-ray study of templated amino acid crystallization was published by Grayer Wolf, Landau, Lahav, Leiserowitz, Deutsch, Kjaer, and Als-Nielsen.[57] Two-dimensional Bragg peaks were observed and a model for headgroup-packing at the interface was generated. Beyond this point, the streams of LM-mineralization and LM-structure determination proceeded in parallel without too much cross-communication for a while. An X-ray study of NaCl crystal formation under films of fluorocarbon amphiphiles was reported, almost as a sidebar within a study of pH- and pressure-dependent film organization.[58] Epitaxial ice under the alcohol LM was also studied with X-rays,[59] and this was noted in the $CaCO_3$ LM literature just mentioned. Beginning in 1990 though, the most attention in the liquid surface scattering community was focused on cation-induced structural reorganization[60–62] and cation binding[61,63] at LM interfaces. There was keen interest in finding the two-dimensional cation superlattices that would support the bidentate Stern layer model, and these were first identified in 1994 in the Cd arachidate system,[63] and further explored in other systems.[64–67] A few of these reports were referred to in the mineralization literature when estimates of the molecular lattices were needed for comparison to mineral crystal structures, but none of these X-ray experiments on divalent cations were conducted under mineral nucleating conditions.

Somehow, it was not until the twenty-first century that structural results on $CaCO_3$–stearate were announced! The two independent groups who conducted them found the same results: unoriented crystals at early nucleation stages; modified stearic acid structure relative to what had been known for films on water; and polytype control not from template structure but from kinetics.[68–70] These findings precipitated a bifurcation in subsequent studies. Work based at Brookhaven National Laboratory asked the question: since film structure is not important in $CaCO_3$ templating, what is? and went on to chime in on the literature of amorphous calcium carbonate films[71–73] and to quantify calcium binding at films, which was subphase-dependent but always reduced compared to the Stern layer model.[68] Kmetko and co-workers at Northwestern University asked: since structural templating does not occur in $CaCO_3$, can we find a system where it does?[70,74–76] Their pursuit of a templated system led to unique results on barium fluoride and directly if unexpectedly to the issue of template adaptability.

The fatty acid–barium fluoride system

Kmetko, Yu, Evmenenko, Kewalramani, and Dutta were the first to identify, with *in situ* X-ray scattering, a system in which oriented mineralization could be correlated to the structure of the two-dimensional Langmuir monolayer template.[74] Monolayers of heneicosanoic acid were prepared on supersaturated barium fluoride solutions at barium concentrations from 3 to 14 mM. Selected data from ref. 74 are reproduced in Fig. 1. At dilute barium concentrations, the cations were found to induce an untilted, approximately hexagonal phase in the monolayer, identified from a single Bragg rod: Fig. 1(a), △. Phase separation occurred in the monolayer at and above concentrations of 3.7 mM, with the appearance of a new set of three peaks in the monolayer scattering pattern: Fig. 1(a), ▲. Because two of these peaks have non-zero surface-normal momentum transfer component, the data indicate a coexisting tilted monolayer phase with a new set of 2D lattice parameters. The organic lattice was found to be independent of barium concentration in this regime.

As the BaF_2 crystals nucleated, the evolution of their lattice parameters and orientation could also be tracked by *in situ* diffraction. The inorganic peaks identified corresponded to a cubic structure with lattice spacings close to that of bulk BaF_2, with the (100) face parallel to the monolayer. Fig. 1(b) shows the {200} BaF_2 peaks measured at the interface for different concentrations. Notably, the mineral phase is strained. The strain decreases such that the lattice reaches the bulk value above 11 mM barium concentration. When the lattice constants were extrapolated to zero barium concentration to extract the early-stage mineral structure, the cubic parameter 5.82 Å was obtained. The corresponding unit cell area of 33.85 Å is 1.50 times that of the measured surfactant lattice, suggesting an epitaxial relationship. A common supercell uniting the two structures is shown in Fig. 1(c). These experiments demonstrated two important facts. First, the template and mineral have the capacity to adapt to each other—a feature which may be crucial for true epitaxial relationships, consistent with the interactions between mineral and monolayer surfaces being strong enough to affect them both. Second, the supercell lines up its single corner atom while leaving 11 fatty-acid headgroups and 15 cations completely displaced from each other. This is not the idealized lattice matching that one imagines would optimize mineral–organic interactions. Whether this kind of epitaxy is at work in biomineralization is still an open question.

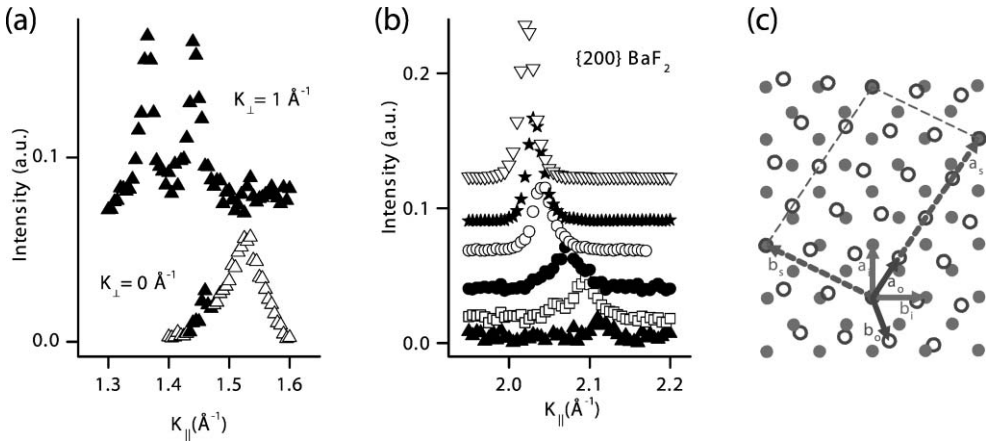

Fig. 1 Data from the fatty acid–BaF_2 system. (a) Coexisting phases of heicosanoic acid monolayers in the presence of barium. △: peak from untilted structure at low concentration. ▲: one on-axis and two off-axis peaks for tilted phase on supersaturated barium fluoride solution. (b) BaF_2 peak showing strain relaxation as a function of salt concentration in mM: ▽, 11.2; ★, 9.3; ○, 8.4; ●, 7.5; □, 5.6; ▲, 3.7. (c) Supercell parameters (a_s, b_s) relating the organic lattice parameters (a_o, b_o) to extrapolated inorganic parameters (a_i, b_i). Reprinted figure with permission from J. Kmetko, C. Yu, G. Evmenenko, S. Kewalramani and P. Dutta, *Phys. Rev. Lett*., 2002, **89**, 186102 (ref. 74). Copyright (2002) by the American Physical Society.

Experimental

To determine its relevance, it is important to probe template adaptability in a more direct way. We have recently described a family of surfactants consisting of a dodecyl chain connected *via* a bisureido-heptylene unit to an amino acid headgroup: glycine-, alanine-, valine-, and leucine- based compounds were reported.[77] These compounds form Langmuir monolayers in which the spacing of molecules along one dimension is expected to be controlled by the hydrogen bonding of adjacent bis-urea units.[78–80] In the previous report we have described the measurements of Langmuir isotherms and infrared spectroscopy, along with the results of mineralization experiments. The GLY and VAL based compounds (referred to as **1** and **3** in ref. 77) were also studied by *in situ* synchrotron X-ray scattering, with preliminary results being published in ref. 77. The GLY and VAL compounds represent two different regimes when used as templates for calcium carbonate mineralization. While the GLY compound efficiently induces calcite mineralization at the interface, no preferred orientation was observed. The VAL compound by contrast effectively nucleated the (100) face. To answer the question of whether molecular recognition, template adaptability, or other mechanisms make the crucial difference between these compounds, it is crucial to obtain experimental information about the template structure, in the presence and absence of cations. In this paper we will describe the detailed analysis of grazing-incidence X-ray scattering and X-ray reflectivity from the VAL and GLY compounds on pure water and 0.01 M $CaCl_2$ subphases, along with results of *in situ* mineralization experiments.

GLY and VAL solutions of 1.0 mg mL^{-1} and 0.5 mg mL^{-1} respectively in 4 : 1 chloroform–methanol were prepared. 50 to 80 μL quantities were dropped from a syringe to spread monolayers on the aqueous subphases at nominal surface coverages (based on previous in-house isotherm data) of 80%. The Langmuir trough, custom built at Brookhaven National Laboratory, consisted of removable Teflon trays of dimension 13.7 × 7.2 cm and 1 cm deep, oriented with the long axis along the incident X-ray beam direction. The trough has a computer controlled barrier for film compression, a cooling block below the trays which maintained liquid temperature at 18 °C, a stainless steel gas-tight housing with kapton (polyimide) X-ray windows, and an oxygen sensor. Subphases used were either Milli-Q water or 0.01 M $CaCl_2$. For experiments on the static subphases, helium gas was flowed through a water bubbler, into the trough, and out through a flow-reducing filter, to prevent carbon dioxide from the air from affecting $CaCO_3$ mineralization, to remove oxygen which would lead to damage of the organic film by the X-ray beam, and to reduce X-ray absorption by the vapor. For mineralization experiments, the trough was purged with helium bubbled through water after preparation of the film. Then the water bubbler was swapped to a solution of 0.01 M $(NH_4)_2CO_3$, warmed in a metal canister with heater tape to 35 °C. Flow of ammonium carbonate gas was routed from the trough through an ice bath, a dessicant drying column, and a CO_2 meter to confirm the gas decomposition. Mineralization runs were monitored using X-ray diffraction for about 12 hours.

X-Ray experiments utilized the BNL/Harvard Liquid Surface Spectrometer at Beamline X22B at the National Synchrotron Light Source, Brookhaven National Laboratory and were performed with X-ray wavelength 1.53 Å. Reflectivity measurements were done using a single channel NaI (Bicron) scintillator detector and slit collimation. Grazing-incidence diffraction (X-ray incidence angle 0.12°) utilized a linear position sensitive detector, with a 10 cm active area oriented vertically, and Soller slit collimation for 0.24° angular resolution in the horizontal scattering angle. Optical microscopy was performed at BNL on crystals collected from the trough after mineralization experiments on glass cover slips. Crystals collected on microscopy grids were returned to Eindhoven for scanning electron microscopy.

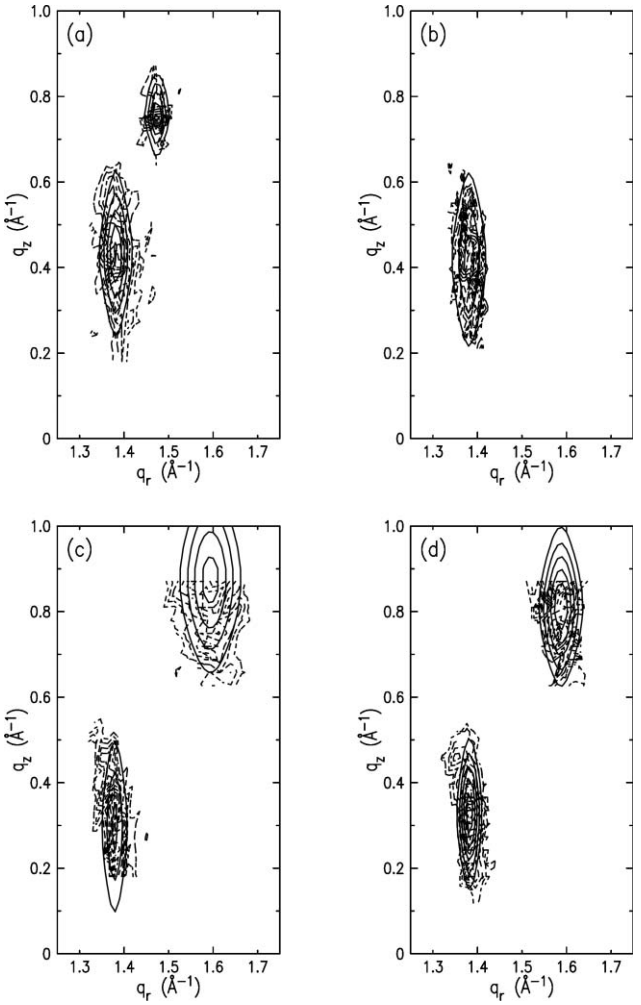

Fig. 2 Grazing-incidence diffraction data shown as background-subtracted intensity contours as functions of in-plane q_r and surface-normal q_z components. (a) VAL, H_2O. (b) VAL, 0.01 M $CaCl_2$. (c) GLY, H_2O. (d) GLY, 0.01 M $CaCl_2$. (---) Experimental intensity contours. (—) Contours from 2D Lorentzian fit peaks.

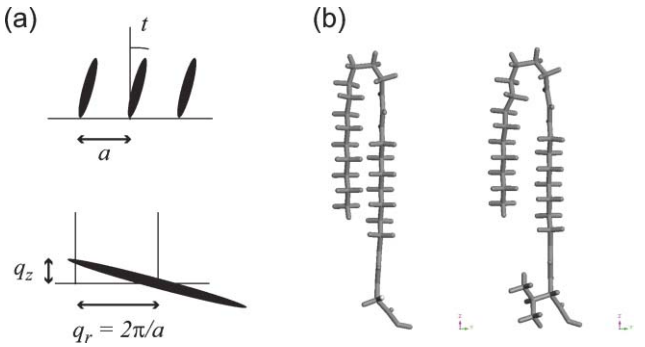

Fig. 3 (a) Top: lattice of rod-shaped molecules with spacing a and tilt angle t relative to the surface-normal. Bottom: map of the corresponding reciprocal space intensity for this structure, with vertical Bragg rods spaced at $2\pi/a$ and molecular form factor intersecting the Bragg rod at $(2\pi/a)$ tan t. (b) Folded molecules for GLY and VAL surfactant molecules, drawn in Accelrys Molecular Modeling software.

Results

Grazing-incidence diffraction

To obtain the most information from grazing-incidence diffraction from Langmuir films, intensity may be resolved in both the in-plane and surface-normal components of the scattered wave-vector, q_r and q_z respectively. We show our data as contour plots of intensity as a function of these wave-vector components in Fig. 2. Data for the VAL and GLY compounds on H_2O and $CaCl_2$ are shown, along with the contours of two-dimensional Lorentzian fits to the data, with the fit parameters in Table 1. The data have the form of Bragg rods, that is, extended along the q_z direction. The averaged observed width in q_z from the fits is 0.31 Å^{-1}, indicating that the peaks arise from a surface layer $\approx 2\pi/0.31 = 20$ Å in thickness, compatible with a Langmuir monolayer. The q_r component of each peak corresponds to an in-plane spacing of rows of molecules, yielding parameters of the two-dimensional lattice. All observed peaks in our system have a non-zero q_z component. This arises when the molecular backbone is tilted relative to the surface normal. The expected diffraction patterns for assemblies of rod-shaped molecules such as fatty acids have been analyzed in detail.[81–83] The relationship between q_r and q_z for the rod-shaped molecule is illustrated in Fig. 3(a), which depicts a lattice of molecules with spacing a tilted by an angle t to the surface normal. The scattering condition from the monolayer film is satisfied along Bragg rods which extend along the surface normal direction in reciprocal space and have spacing $2\pi/a$. The rod-shaped molecule has a pancake-shaped form factor, which for finite tilt, intercepts the Bragg rods at finite values of q_z. For such a structure, the diffracted intensity will be maximum at a value $q_r = 2\pi/a$, which determines the in-plane lattice constant, and $q_z = q_r$ tan t, which determines the molecular tilt. When more than one peak is observed, they must be indexed according to a consistent two-dimensional film structure.

Our surfactant assemblies are expected to be less symmetrical than an array of fatty-acid like molecules, due to H-bonding between bis-urea units. This informs our interpretation of the diffraction peaks. First we note that for both

Table 1 Parameters from two-dimensional Lorentzian fits to the grazing-incidence diffraction data from VAL and GLY films on H_2O and 0.01 M $CaCl_2$ subphases. Values and uncertainties from least squares fitting are rounded to the second decimal place

	Peak 1 parameters/Å^{-1}				Peak 2 parameters/Å^{-1}			
	q_r cen	q_r FWHM	q_z cen	q_z FWHM	q_r cen	q_r FWHM	q_z cen	q_z FWHM
VAL H_2O	1.38 ± 0.00	0.05 ± 0.00	0.43 ± 0.01	0.27 ± 0.02	1.47 ± 0.00	0.04 ± 0.01	0.76 ± 0.01	0.12 ± 0.03
VAL $CaCl_2$	1.38 ± 0.00	0.06 ± 0.00	0.42 ± 0.01	0.33 ± 0.02	—	—	—	—
GLY H_2O	1.38 ± 0.00	0.05 ± 0.00	0.30 ± 0.01	0.38 ± 0.02	1.59 ± 0.00	0.14 ± 0.03	0.87 ± 0.05	0.45 ± 0.13
GLY $CaCl_2$	1.38 ± 0.00	0.05 ± 0.00	0.33 ± 0.01	0.32 ± 0.02	1.59 ± 0.00	0.09 ± 0.01	0.81 ± 0.02	0.32 ± 0.07

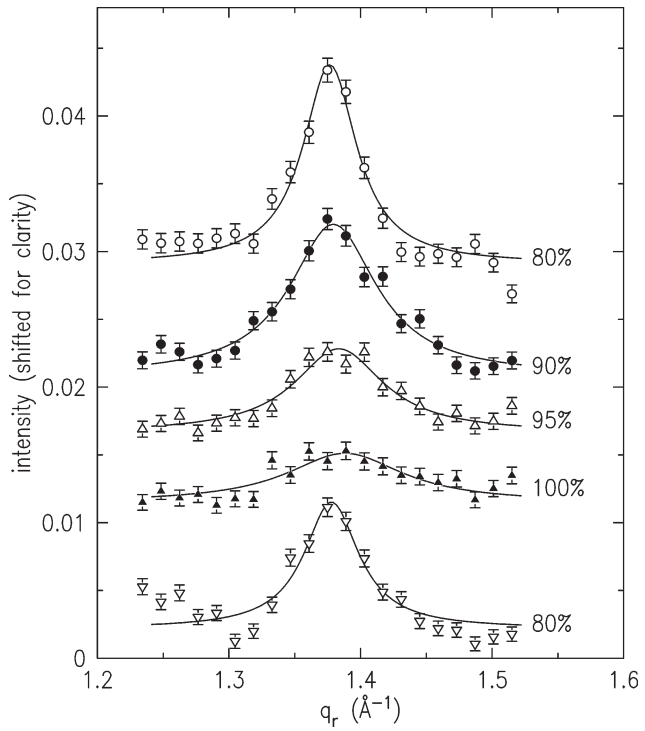

Fig. 4 In-plane diffraction data for the H-bonding peak of VAL on H_2O, showing the effect of surface pressure. The film is initially spread at nominal 80% coverage (○). Reduction of surface area in the Langmuir trough, increasing the coverage to 100%, broadens and weakens the peak without changing its position. The peak recovers almost completely when the pressure is reduced by returning surface area to the 80% coverage value (▽).

compounds under all conditions, Fig. 2 shows a primary peak with q_r = 1.38 Å^{-1}. The corresponding lattice spacing is a = 4.55 Å, exactly as expected for hydrogen-bonded units. Whether on the H_2O or $CaCl_2$ subphase, the q_z component is ≈0.4 and 0.3 Å^{-1} for the VAL and GLY compounds respectively, which can be interpreted simply as tilts of 17° and 12° along the bonding direction. Hence the molecular structure is built up from H-bonded molecular ribbons, as anticipated. From the q_r peak widths, correlation lengths of about 125 Å, or about 28 molecules per linear domain, can be estimated. Additional supporting evidence for our interpretation is obtained by the application of surface pressure, shown as a two-dimensional plot (summed over linear detector channels in the q_z direction) for the VAL compound on water in Fig. 4 (with fit parameters for the 3D data set in Table 2). Surface pressure changes leaves the q_r peak position unchanged within the statistics of our fits, but the amplitude decreases markedly as the nominal surface coverage is increased from 80% to 100%. Upon expanding the trough area back to 80% coverage, the amplitude returns to 2/3 its original value. The q_z component as seen in Table 2 increases slightly with pressure, indicated a possible increased tilt of 2°. We conclude that the H-bonds have no capability to change their length, instead, too much compression causes the ribbons to break apart. The tilted molecules, instead of standing upright, may become slightly sheared as pressure is applied to the assembly.

The observation of a second peak can be interpreted in more than one way. It can be another reciprocal lattice vector in the 2D lattice, or it can appear due to phase coexistence, representing a molecular spacing in a second phase. Assigning a structure based on only one or two peaks is not a sure analysis, but is often necessary in the case of Langmuir films lacking significant long-range order to diffract at higher orders. In our case, we continue our analysis making use of chemical information. We note that a second peak is observed *only on water* for the VAL compound, but on *both subphases* for the GLY compound. In addition, the peak lies at a greater q_r value, representing a smaller lattice spacing, for the GLY compound than for the VAL compound. Both these points are consistent with the second peak defining an orthogonal degree of order in the films, with some independence possible between them. This second spacing depends on headgroup size in the expected way, with the greater VAL headgroup defining a spacing of b = 4.27 Å between H-bonded molecular ribbons. The inter-ribbon distance is b = 3.95 Å for the GLY system, unaffected by calcium. At this point we still have not defined whether we envision a rectangular lattice of molecules, with the two lattice vectors perpendicular to each other. Under this assumption, the unit cell area would be 19.4 Å^2 for the VAL compound and 18.0 Å^2 for the GLY compound. These numbers are inconsistent with those obtained from Langmuir isotherms, which yielded mean molecular areas of 34 and 27 Å^2 per molecule for the two compounds. Furthermore, the q_z components of the second peaks imply tilts of 27–29°, which also must be explained. With grazing-incidence diffraction alone, it would be difficult to draw conclusions about the template structure.

Reflectivity

Further structural information is available, however, from the X-ray reflectivity. The reflectivity is a probe of the surface-normal electron density profile $\rho(z)$, and is capable of sub-Ångstrom resolution. In the kinematic limit, the reflectivity normalized by the Fresnel reflectivity R_F of a flat water surface with density ρ_0 is written:

$$R(q_z)/R_F = \left| \frac{1}{\rho_0} \int (\partial\rho/\partial z) \exp(iq_z z) \mathrm{d}z \right|^2,$$

Table 2 Parameters from two-dimensional Lorentzian fits to the VAL peak 1 under compression. Values and uncertainties from least squares fitting are rounded to the second decimal place. Parameters in Å^{-1} except for peak amplitude in arbitrary units

Coverage (%)	q_r cen/Å^{-1}	q_r FWHM/Å^{-1}	q_z cen/Å^{-1}	q_z FWHM/Å^{-1}	Amplitude
80 initial	1.38 ± 0.00	0.06 ± 0.01	0.41 ± 0.01	0.34 ± 0.03	6.9 ± 1.2
90	1.38 ± 0.00	0.06 ± 0.01	0.45 ± 0.01	0.30 ± 0.05	3.8 ± 1.0
95	1.37 ± 0.00	0.06 ± 0.02	0.47 ± 0.02	0.31 ± 0.07	2.4 ± 1.0
100	1.37 ± 0.01	0.07 ± 0.02	0.48 ± 0.02	0.25 ± 0.07	1.5 ± 0.8
80 final	1.38 ± 0.00	0.06 ± 0.01	0.41 ± 0.01	0.32 ± 0.04	4.6 ± 1.0

and a model film profile $\rho(z)$ can be determined and its computed reflectivity refined against the data. In our previous report,[77] we described the results of free fits of a "slab model", in which $\rho(z)$ was built from two arbitrary slabs of parameterized thickness and density, and refined freely without constraint for the VAL–H_2O reflectivity data. From that free fit a film thickness of about 20 Å was extracted. This result agrees with the q_z widths of the grazing-incidence Bragg peaks, discussed above. Notably, it is *inconsistent* with a model in which the compounds have straight, extended hydrocarbon tails above the water—the molecules would be nearly 30 Å long. The reflectivity fit also provides a mean molecular area, since the number of electrons per molecule and per $Å^2$ in the model density profile are both known. We reported an average surface area per VAL molecule on water as 37 $Å^2$. This is truly excellent agreement with the Langmuir isotherm value of 34 $Å^2$, being a completely independent measurement. The slightly larger value can easily be due to the presence of gaps between domains, or loss of material to the subphase, which is averaged over in the reflectivity measurements.

All of our experimental observations can be reconciled if the molecular tails are folded over as shown in Fig. 3(b). In this model, the in-plane lattice is determined by the alternating close-packed bisureido-heptylene backbones and alkyl tails. The unit cell area per molecule from the diffraction pattern becomes 38.8 and 36.0 $Å^2$ for the VAL and GLY compounds respectively. The isotherm and free-fit reflectivity data (which unlike the diffraction are dependent on assumptions of uniform surface coverage) are now quite close to these values. The folded tails also yield a film thickness closer to 20 Å.

In the present paper, we investigate the reflectivity data in more detail using these folded molecules as a starting point. We model the reflectivity data not by homogeneous density slabs, but using the depicted molecules, drawn in the Accelrys Materials Modeling software. A lookup table in the software (the "clean" tool) creates reasonable interatomic spacings in the chains. The alkyl tails were folded over close to the upper bis-urea unit, keeping the backbone straight but otherwise making the molecule as short as possible as a test of the molecular tilts indicated by in-plane diffraction. The model was exported as a file of atomic z-positions, which were represented as a table of Gaussians to make up the model $\rho(z)$. Refinement parameters were: a tilt angle t for the entire folded molecule, which compresses the z-positions by the factor cos t; a z-offset relative to the subphase boundary; a mean molecular area; and a Gaussian broadening for the atomic positions. The broadening factors were always in the range 6–8 Å, with no systematic dependences. The offset parameter always placed the lowest atom in the molecule 2 Å towards the vapor, relative to the liquid interface position. An additional atomic term for Ca^{2+} was included in certain fits, with independent concentration and z-position. Both of the z-coordinates, that for the molecule and that for the Ca^{2+} cation, were refined in fits and also forced at selected values to explore the possible variability. The z-offset of the molecule and the z-position of the cation can be moved by no more than 1 Å from the reported values in fitting the data. Error bars from least squares fitting, when these parameters are refined, are generally a few tenths of an Ångstrom.

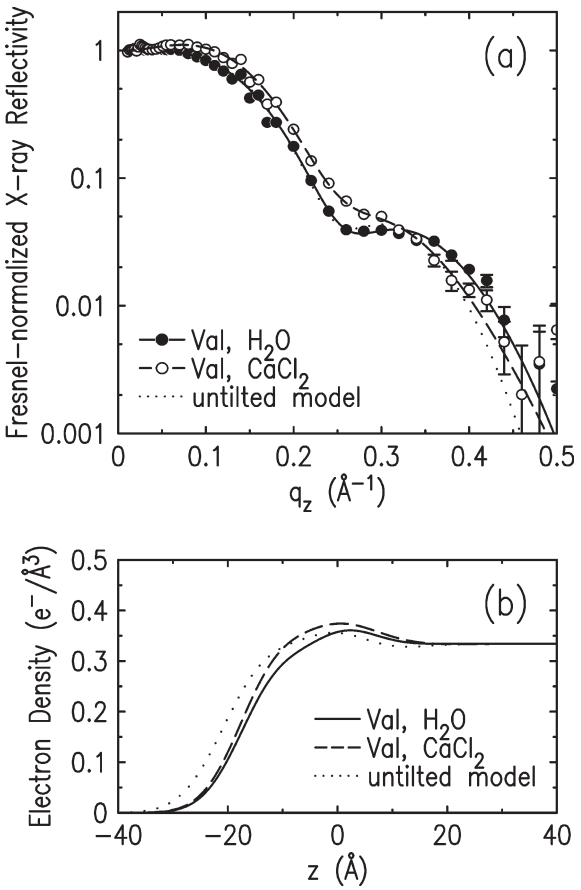

Fig. 5 (a) Fresnel-normalized reflectivity data for VAL on H_2O (●) and 0.01 M $CaCl_2$ (○). Lines through the experimental points are calculated reflectivity curves from models based on folded surfactant molecules at the surface. (b) Model surface-normal density profiles corresponding to the reflectivity fits shown in (a). (—) Best fit model for VAL on H_2O. (---) Best fit model for VAL on $CaCl_2$. (.....) A model of folded but untilted molecules defines a film a few Å thicker than the best fit models in (b), and misses the experimental reflectivity points as shown in (a).

Fig. 5(a) shows reflectivity data and fit curves for the VAL compound on H_2O and 0.01 M $CaCl_2$. In panel (b) are real-space model density profiles, showing the subphase at $z > 0$ and the region where the molecule sits at the interface. First we investigated whether the folded molecules can be upright on the surface. As the dotted line shows, an untilted molecule misses the oscillation period in the reflectivity; such a film is slightly too thick to be consistent with the data. When we allowed the molecule to tilt, this parameter co-varied with the molecular area and could not be fit precisely. Reasonable results were obtained only for tilts from 22–30°. We note that the two tilts from in-plane diffraction peaks are 17.3° and 27.3° for the VAL compound on water. If both these tilts are applied in orthogonal directions, this is equivalent to an overall tilt of 30°, so we fixed the tilts to 30° in subsequent fits to explore calcium binding. The reflectivity data for the VAL compound on $CaCl_2$ could not be modeled by the surfactant without calcium. Parameters for Ca^{2+} cations at the interface were fit for both data sets. We verified that fits to the data taken on water could not be improved by adding the calcium term; the

concentration refined to zero. For the VAL compound on $CaCl_2$, we found a Ca^{2+} concentration of 0.9 ± 0.3 per molecule. The *z*-position of the cation needed to be about 7 Å towards the vapor interface, in other words, about 5 Å above the lowest headgroup atom in the model. This is evidence for Ca complexation by the VAL compound.

The reflectivity data for the GLY compound, shown in Fig. 6, are much more difficult to analyze. The GLY compound is effectively nothing more than a set of close-packed alkyl tails, which have an electron density almost the same as that of water. Contrast from GLY on water is very slight, so there is little constructive interference, and the apparent oscillations are actually very noisy. Nevertheless we have some confidence from fitting that, just as in the case of VAL, the data cannot be described unless the molecule is tilted by about 30°. Addition of calcium improves the situation. Oscillations are now present, because of the electron contrast provided by the cations. Since the molecule still blends into the subphase, fitting is less sure and different choices of constraints yielded Ca^{2+} concentrations of 1.9 ± 0.9 and 1 ± 2. Therefore, the degree of cation binding may be about the same for the GLY and VAL compounds. But a very interesting difference between the two is observed in the cation *z*-position. For the GLY compound, the Ca^{2+} is located 2 Å towards the *subphase* rather than the vapor. This points to a key difference between the interactions between Ca^{2+} and the VAL *versus* GLY compounds. While the VAL headgroup appears to undergo complexation with the calcium within its headgroup region, the GLY compound is better described as attracting an electrostatic layer beneath it. We will return to an elaboration of the film structure in the Discussion section.

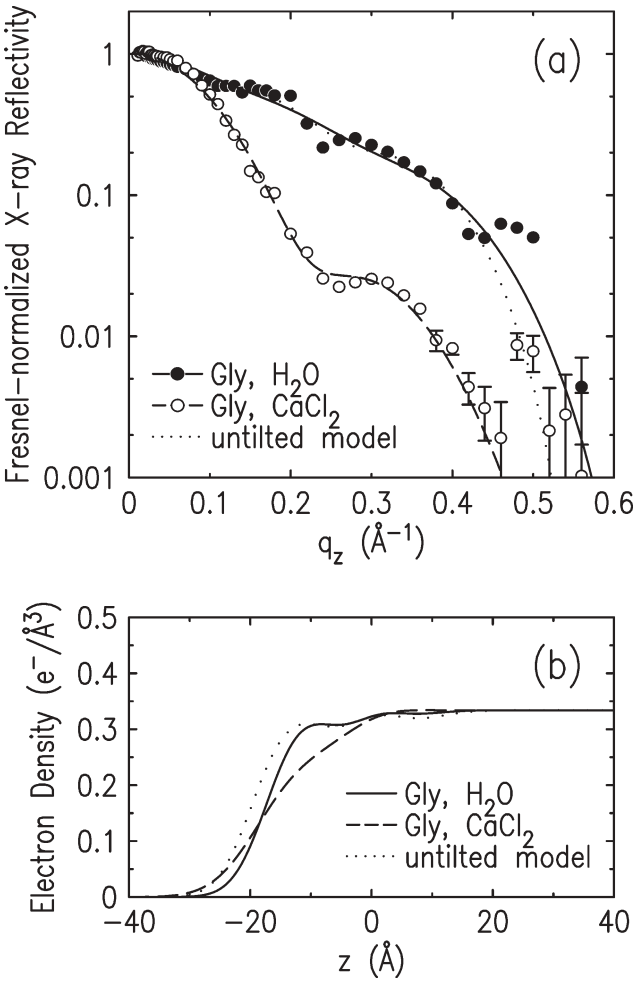

Fig. 6 (a) Fresnel-normalized reflectivity data for GLY on H_2O (●) and 0.01 M $CaCl_2$ (○). Lines through the experimental points are calculated reflectivity curves from models as described in the text. There is very little contrast for GLY on H_2O because the molecule has nearly the same electron density as water. (b) Model surface-normal density profiles corresponding to the reflectivity fits shown in (a). (—) Best fit model for GLY on H_2O. (---) Best fit model for GLY on $CaCl_2$. (.....) A model of folded but untilted molecules.

Mineralization experiments

Previous experiments revealed that the VAL compound modified 70% of calcite crystals to display a concave indentation defined by three roughened planes.[77] Young crystals extracted for transmission electron microscopy revealed (100) diffraction patterns suggestive of nucleation at that face. In those previous experiments, monolayers were spread on freshly prepared supersaturated (≈9 mM) calcium bicarbonate solution in crystallization dishes or a KSV Minitrough and permitted to outgas. In the present work a different mineralization method was chosen to provide more control over the mineralization rate. VAL and GLY films were mineralized in the 0.01 M $CaCl_2$ subphase by the flow of helium gas bubbled through 0.01 M $(NH_4)_2CO_3$ solution, warmed to 35 °C. During the course of mineralization, monitored for 8 to 20 h, the reflectivity and grazing-incidence diffraction patterns were measured at approximately one to two hour intervals.

Our first observation is that the films quickly roughened during mineralization. This can be seen in the in-plane diffraction raw data, shown for VAL in Fig. 7. The figure shows a very wide scattering angle range (not converted to in-plane momentum transfer q_r), integrated over all linear detector channels (that is, approximately integrated over all q_z values). There are three main features in the data: the surfactant H-bonding peak at 19.4 degrees 2Θ, marked with the arrow; a broad hump from 24 to 28 degrees 2Θ which increases with time during mineralization; and sharp Bragg peaks demonstrating that mineralization takes place at the surface. The broad feature can be assigned to the structure factor of bulk water. In the first scan, at grazing incident angle 0.12°, the film is smooth and diffraction from bulk water is prevented by total external reflection of X-rays from the surface. When the film becomes rough, the grazing incidence condition is no longer satisfied, since the X-rays impinge upon regions of the surface which are locally at steeper angles. The result is that successively more bulk water scattering occurs, as the data at longer mineralization times show. This background quickly swamps the monolayer peak, although analysis of this region for the first two scans shows that the H-bond peak is unchanged except for broadening. Likewise, the reflectivity taken *in situ* is interrupted by the roughening and becomes difficult to analyze, though it does increase in intensity at low q_z consistent with the accumulation of dense material at the

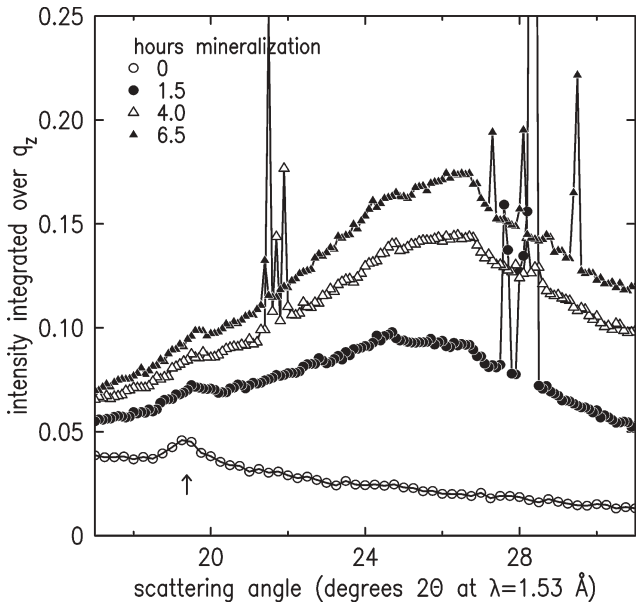

Fig. 7 Raw in-plane scattering data from VAL film being mineralized for 0 to 6.5 h. Arrow marks position of surfactant H-bonding peak, observable mainly in the first scan (○). Subsequent mineralization (●,△,▲) causes surface roughening which increases the background scattering from bulk water. Sharp peaks are calcite Bragg peaks. Data are shown integrated over vertical linear detector counts as function of scattering angle 2Θ.

surface (data not shown). The situation is similar for GLY. We propose that this accumulation of dense but non-diffracting material may point to the formation of amorphous calcium carbonate, which has been indicated as a transient precursor phase both in biological[84] and in biomimetic[85] systems. Neither the sparse coverage of crystals nor the monolayer itself can account for the observations of roughness.

The crystals resulting from these experiments were examined by optical and scanning electron microscopy and showed that the VAL and GLY systems behave differently. On the VAL film, optical micrographs show an abundance of tablets with the rhombohedral calcite morphology (Fig. 8(a)). SEM micrographs (Fig. 8(b)) show that many of these crystals have modified faces displaying the concave (100) depressions described in ref. 77 although some other random modifications as well as a few spherulites with the appearance of vaterite were also observed. In the presence of GLY, $CaCO_3$ forms primarily as calcite polycrystals (Fig. 8(c,d)). Far fewer single-crystal tablets are found, though some of these do have modified faces. It is clear from this survey that although mineralization conditions in the synchrotron setup have not been optimized for habit selection in the same way as the more extensive in-house studies described previously, the VAL film changes the process by which the calcite crystals grow.

From *in situ* surface diffraction we can monitor crystal structure and orientation during mineralization. Representative data shown as contours in q_r and q_z are displayed in Fig. 9 for both VAL (a) and GLY (b). The magnitude $q=\sqrt{q_r^2+q_z^2}$ identifies the *d*-spacing which is indexed for phase identification, while the ratio q_z/q_r is the tangent of the angle this crystal axis makes with the water

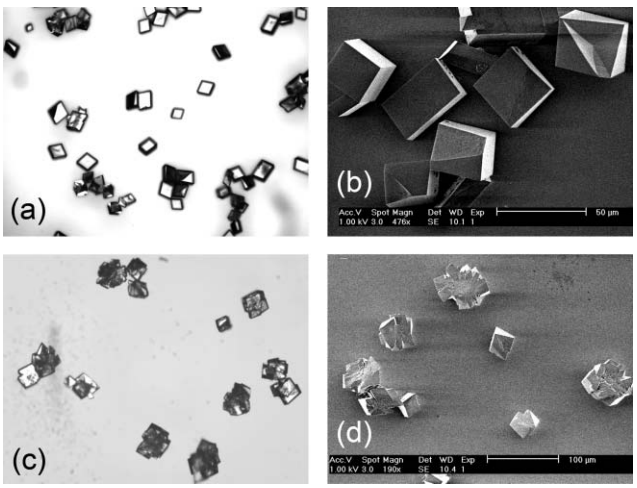

Fig. 8 (a) Optical micrograph of crystals nucleated at VAL film. Predominantly, rhombohedral calcite tablets are observed, field width: 800 μm. (b) Scanning electron micrograph of calcite nucleated on VAL, illustrating numerous modified faces. Scale bar: 50 μm. (c) Optical micrograph of particles nucleated at GLY film: polycrystalline calcite, with roughly spherical aspect ratio, field width: 800 μm. (d) SEM micrograph of particles from GLY film. Many particles have a spherulitic core with a needle-like texture, suggestive of vaterite. Scale bar: 100 μm.

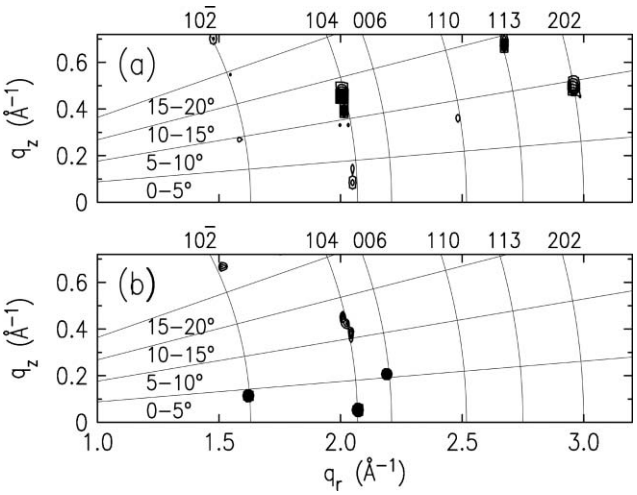

Fig. 9 Contour plot of grazing-incidence diffraction intensity taken from (a) VAL and (b) GLY films during 12 hour mineralization runs. As is typical of all data sets, a selection of calcite Bragg peaks is observed. The peak position resolved in q_r and q_z provides information about the orientation of the [*HKL*] axis as well as the peak indexing. Calcite peaks lie along the labeled arcs of constant q magnitude. The tilt of the *HKL* axis above the water surface plane can be assigned to a range of angles between 0 and 20°, demarcated by the radiating lines.

surface. Indexed arcs in the figure show where accessible calcite Bragg peaks lie. The radiating lines demarcate regions of tilts of 5, 10, 15, and 20 degrees from the surface as labeled. Each of the resolution-limited peaks comes from a separate crystallite in the beam. In exactly one of the observed scans for VAL, a ring pattern for vaterite was seen, consistent with the observation of spherulites by microscopy and showing that one such particle was captured in the beam.

Table 3 Occurrences of calcite Bragg peaks in grazing-incidence diffraction scans, in four angular ranges corresponding to the direction of the indicated [*HKL*] axis relative to the surface plane. Data come from 30 scans each for VAL and GLY films taken over 12 hour mineralization runs. Calcite nucleated on VAL has more (104) peaks in the 10–15° range, due to the flattened tablet morphology

Film	Axis tilt/°	(10$\bar{2}$)	(104)	(006)	(110)	(113)	(202)	Total
VAL	0–5	0	8	1	5	2	2	18
	5–10	3	4	1	2	2	13	25
	10–15	0	29	0	2	5	9	45
	15–20	5	7	0	0	0	—	12
GLY	0–5	2	7	2	3	4	7	25
	5–10	2	12	1	3	4	0	22
	10–15	1	10	2	1	3	7	24
	15–20	1	15	0	1	2	—	18

For each monolayer we performed a 12 hour mineralization run from which 30 diffraction frames were extracted, at successive times and at three different positions on the film surface (*i.e.* the sample was translated under the beam by a few mm between scans). Casual inspection of these figures leads to no obvious conclusions regarding either preferred orientation or time dependence. For each pattern we counted the occurrences of the indicated Bragg peaks within the four tilt-angle ranges shown. The results are collected in Table 3. The main observation from this table is that the VAL-nucleated crystals have a spike of calcite (104) peaks in the 10–15° tilt range, while all other data in the table are comparable. This can be explained simply by the morphology observed. The flat calcite tablets nucleated by VAL have their broad cleavage face parallel to the surface, due to surface tension. The obtuse plane angle between adjacent {104} planes is 102°, or 12° greater than the 90 degree angle between the water plane and the surface normal. In other words, as long as a rhombohedral calcite crystal is lying with a face parallel to the water interface, there will be a [104] vector which points upwards 12° from the surface plane, which is captured by the detector at the q_r and q_z values indicated. This effect is not observed for GLY because there is no force orienting the rounded polycrystals in any particular way.

Discussion

We return to a discussion of the model structures for the two mineralization templates. We have argued that the molecular spacing of 4.55 Å along one dimension is due to H-bonding between neighboring bis-urea units, with a tilt of 12° for GLY and 17° for VAL along this direction. Without the molecular tilt, the backbones would be parallel, as indicated in Fig. 10(a), with bifurcated hydrogen bonding between the C=O and the pair of N–H groups indicated by the dashed lines. With the tilt, these bonds are disrupted, as Fig. 10(b) and (c) show for GLY and VAL respectively. In these cases only one of the N–H groups is in reach to form the hydrogen bond to its neighbor. It should be noted that at present there is no indication, from FTIR data acquired on Langmuir–Blodgett films removed to solid substrates, that this is the case.[77] Therefore to justify this energetically, it would be necessary to investigate this further taking into account not only the interactions between

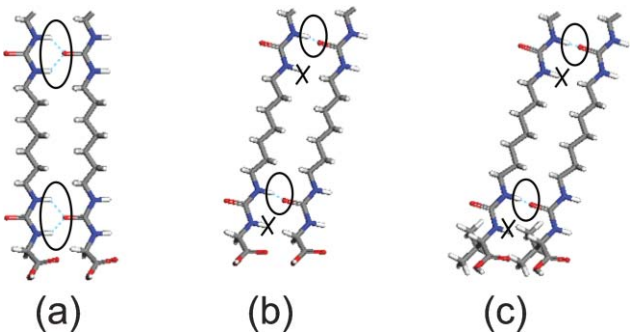

Fig. 10 (a) Model GLY molecules aligned with parallel backbones orthogonal to their bonding direction, creating optimal H-bonding between bis-urea units. The bond is disrupted for the 12° tilt of GLY (b) and the 17° tilt of VAL (c) determined from diffraction data. Molecules were rendered in Accelrys Materials Modeling software and annotated using Adobe Illustrator.

hydrocarbon tails which drive the structure, but the subphase interactions as well. Computational work in this direction could be pursued to demonstrate that this model is chemically reasonable. The X-ray diffraction data are unequivocal that this tilt exists along a direction with 4.55 Å spacing. Perhaps the rather short correlation length of 125 Å supports the view that the structure is a compromise between optimal H-bonding and the competing interactions at the water interface, since bulk bis-urea based compounds with long-range 3D crystallographic order and presumably parallel backbones have been reported elsewhere.[78–80] From investigations of silica networks containing asymmetric bis-urea fragments, one of us (B.P.P.) found C=O···H–N distances of 1.88 and 2.1 Å.[86] In the structures we depict here, the corresponding short and long C=O···H–N distances for VAL are 1.01 and 2.82 Å, and for GLY 1.20 and 2.45 Å. Perhaps a twist in the structure, undetectable by our measurements, brings these H-bonds into more reasonable alignment.

Our model structure is thus assembled from adjacent ribbons of molecules bonded along the *x*-direction. The alkyl tails are folded between neighboring ribbons in the *y*-direction, and the deeper corresponding tilt in this second direction as shown in Fig. 11. In this case the tilt is physically reasonable: it creates a larger overlap between the tails and backbones by bringing the tails closer to the interface. X-Ray studies show that most phases of fatty acid like molecules adopt tilts of up to 30° in Langmuir monolayers, except at the highest surface pressures.[82] Note that we depict the headgroup conformations which were used for fitting, but we have no evidence for these in detail. The 6–8 Å roughness of the films makes it hard to explore the structure at higher resolution.

In-plane ordering of the headgroups, which would double the unit cell, should have created additional diffraction peaks, which we did not observe. Hence the headgroups are probably disordered in their layer at the surface. Finally, we could consider alternatives to a rectangular cell, for example a twist of the fold which creates hexagonal or herringbone packing of the hydrocarbon backbones and tails. However, lacking more than two diffraction peaks, we would not be able to distinguish among additional models. For this reason, our sketch of the *x*–*y* projection in Fig. 11 shows the simple rectangular

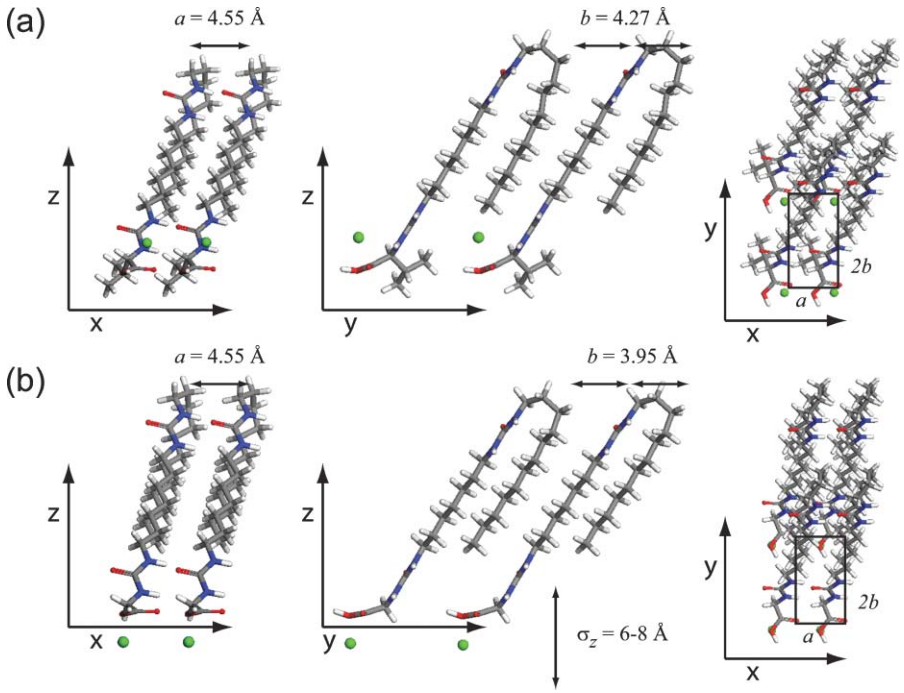

Fig. 11 Projections of structural model showing how (a) VAL and (b) GLY monolayers are assembled. In the *x*–*z* and *y*–*z* projections, the horizontal axis ($z = 0$) lies along the water interface. The parameterized *z*-coordinates of the Ca cations (balls) are shown. The *a* and *b* parameters correspond to the lattice of alkyl backbones and tails. The $a \times 2b$ unit cell contains one surfactant molecule. The roughness σ_z extracted from reflectivity fits is indicated by the double-headed arrow at bottom and represents the magnitude of corrugation or variation in *z*-position of the molecules across the entire film. Molecular models were drawn in Accelrys Materials Modeling software and exported to Adobe Illustrator for annotation.

packing. The $a \times b$ unit cell from diffraction arises from the alternate backbones and tails, and the $a \times 2b$ cell contains one surfactant molecule. Although the figure shows an ordered cell of calcium cations in the rectangular lattice, we note again that the lack of superstructure peaks argues against such crystallographic order. Our data suggest merely that on average, one cation per molecule is associated with the film–water interface.

The relative *z*-positions of the cations, modeled in reflectivity analysis for the films on $CaCl_2$, indicate that calcium is complexed up into the headgroup region for the VAL compound, while it collects below the headgroups for the GLY compound. We believe that this may be the first demonstration of the difference between cation complexation and cation physisorption at two otherwise similar Langmuir monolayer mineralization templates. Another key difference between the VAL and GLY compounds is the GLY system retains essentially the same structure whether assembled on pure water or in the Ca^{2+} bearing subphase. The VAL compound on the other hand exhibits the remarkable property of releasing its 2D order when in the presence of calcium. We presume that this property is connected to the difference in cation position between the two compounds, since in principle the carboxylates of both compounds might be expected to interact with the calcium in the same way. We propose that by keeping the neighboring surfactant ribbon slightly further away, the VAL headgroups give themselves more flexibility to reorient in the way most favorable to cation complexation. By contrast the GLY film structure is dominated by alkyl tail packing and there is either no flexibility or no space for cations to move above the interface layer.

This would have seemed a rather extreme measure of template ''adaptability'' had it been designed into the monolayer deliberately, but experiments confirm that the VAL compound can selectively nucleate the (100) face of calcite. Here, arguments of a lattice match have no referent. Instead, the VAL compound may simply have the ability to collect cations and make them available exactly as the crystal nuclei may need for a face with a given cation density. We also noted previously[77] that a number of calcite-nucleating films seem to share a motif of 4.5–4.6 Å spacings of functional groups which are driven by H-bonded units. Perhaps what is required is a *lack* of interference from a strict organic structure in the orthogonal direction. This is an interesting future direction to explore and could be probed by further specific design of organic template molecules, and by computational studies.

In these experiments VAL induces the formation of indented crystals similar to those we have reported previously.[77,87] We have proposed in the previous work that the indentations result from the effect of the monolayer in hindering transport of Ca^{2+} and HCO_3^- to the selected crystal face as it grows.[87] As the crystal becomes heavier and pulls downward away from the film, the flexible monolayer can follow to a certain extent. The bending of the film will create gaps at the crystal edges, where ion transport will be more effective. The crystal edges will grow faster than the center, producing indentations. The reason that the X-ray diffraction data do not demonstrate alignment of large calcite crystals with the (100) face parallel to the interface is likewise related to the fact that the bulk crystal alignment is determined by gravity and surface tension. The initial (100) faces are small, and soon after their formation the

surface of the crystal becomes dominated by other, more stable faces. These other faces will lie parallel to the monolayer. Especially since the (100) faces are present in threefold groups on indented surfaces, these faces clearly cannot lie parallel to the interface for the bulk crystal.

Our experiments provide information about several steps of the growth of the modified calcite crystals. We prove here that the VAL template reorganizes at first in the presence of calcium. This capability to reorganize was argued to be important if an organic film must recognize a crystal. Next, we believe it is possible that short-lived calcium carbonate precursor phases may be forming, but there is no evidence that the monolayer organization affects this. We do know that VAL monolayers nucleate selected calcite faces while GLY films allow rhombohedral polycrystals to form. Further crystal growth in both systems follows the morphology of calcite in solution, and is not directly affected by the organic species. Therefore, template adaptability can only be relevant in certain of the steps of the growth of our crystals: the reaction to calcium cations, which can affect local charge distributions and ion transport, and the capability to stabilize (001) calcite faces. Future experiments on a variety of systems will undoubtedly clarify where this concept of template adaptability belongs among others, and its role in biomineralization.

Conclusions

We have studied the structure of two examples of a family of adaptable monolayer templates for mineralization. *In situ* X-ray studies were of critical importance in determining the template structures, which differ appreciably from what may have been drawn as a model in the absence of such data—raising a number of fascinating new questions. We confirm that an H-bonded design, combined with tunable valine- or glycine-based headgroups, creates a system of related compounds in which the precise qualities relevant to mineralization can be identified. The larger VAL headgroup makes the monolayer sufficiently flexible so that in the presence of calcium, it can completely release a structural constraint in one dimension, which retaining an obviously relevant molecular spacing in another. In mineralization studies, the VAL film nucleates rhombohedral calcite tablets with modified faces. By contrast an otherwise similar GLY-based film does not change its structure upon exposure to calcium, and resulting calcite particles are polycrystals surrounding a spherulitic core. We speculate that the effective 1D order and H-bond controlled spacing in the VAL film has essential similarities to the protein-based organic matrices in living organisms (which are comparatively disordered on long length scales) which direct biomineralization.

References

1 S. A. Gordziel, D. R. Flanagan and J. Swarbrick, *J. Colloid Interface Sci.*, 1982, **86**, 178.
2 E. M. Landau, M. Levanon, L. Leiserowitz, M. Lahav and J. Sagiv, *Nature*, 1985, **318**, 353.
3 L. Addadi, J. Moradian, E. Shay, N. G. Maroudas and S. Weiner, *Proc. Natl. Acad. Sci. USA*, 1987, **84**, 2732.
4 P. Dutta, J. B. Peng, B. Lin, J. B. Ketterson, M. Prakash, P. Georgopoulos and S. Ehrlich, *Phys. Rev. Lett.*, 1987, **58**, 2228.
5 S. Mann, B. R. Heywood, S. Rajam and J. D. Birchall, *Nature*, 1988, **334**, 692.
6 S. Mann, B. R. Heywood, S. Rajam and J. D. Birchall, *Proc. R. Soc. London, Ser. A*, 1989, **423**, 457.
7 S. Rajam, B. R. Heywood, J. B. A. Walker, S. Mann, R. J. Davey and J. D. Birchall, *J. Chem. Soc., Faraday Trans.*, 1991, **87**, 727.
8 J. B. A. Walker, B. R. Heywood and S. Mann, *J. Mater. Chem.*, 1991, **1**, 889.
9 B. R. Heywood, S. Rajam and S. Mann, *J. Chem. Soc., Faraday Trans.*, 1991, **87**, 735.
10 B. R. Heywood and S. Mann, *J. Am. Chem. Soc.*, 1992, **114**, 4681.
11 B. R. Heywood and S. Mann, *Langmuir*, 1992, **8**, 1492.
12 B. R. Heywood and S. Mann, *Adv. Mater.*, 1992, **4**, 278.
13 S. Mann, D. D. Archibald, J. M. Didymus, T. Douglas, B. R. Heywood, F. C. Meldrum and N. J. Reeves, *Science*, 1993, **261**, 1286.
14 B. R. Heywood and S. Mann, *Chem. Mater.*, 1994, **6**, 311.
15 B. R. Heywood and S. Mann, *Adv. Mater.*, 1994, **6**, 9.
16 R. J. Davey, S. J. Maginn, R. B. Steventon, J. M. Ellery, A. V. Murrell, J. Booth, A. D. Godwin and J. E. Rout, *Langmuir*, 1994, **10**, 1673.
17 H. B. Lu, C. L. Ma, H. Cui, L. F. Zhou, R. Z. Wang and F. Z. Cui, *J. Cryst. Growth*, 1995, **155**, 120.
18 J. Yang, F. C. Meldrum and J. H. Fendler, *J. Phys. Chem.*, 1995, **99**, 5500.
19 J. Yang and J. H. Fendler, *J. Phys. Chem.*, 1995, **99**, 5505.
20 K. C. Yi and J. H. Fendler, *Synth. Met.*, 1995, **71**, 2109.
21 R. Tang, Z. Tai and Y. Chao, *J. Chem. Soc., Dalton Trans.*, 1996, 4439.
22 R. Tang, Z. Tai and Y. Chao, *Chem. Lett.*, 1996, 535.
23 R. Tang, C. Jiang and Z. Tai, *J. Chem. Soc., Dalton Trans.*, 1997, 4037.
24 R. Tang, C. Jiang and Z. Tai, *J. Chem. Soc., Faraday Trans.*, 1997, **93**, 3371.
25 C. Jiang, R. Tang and Z. Tai, *J. Mater. Chem.*, 1998, **8**, 81.
26 J. Lahiri, G. Xu, D. M. Dabbs, N. Yao, I. A. Aksay and J. T. Groves, *J. Am. Chem. Soc.*, 1997, **119**, 5449.
27 B. Li, Y. Liu, N. Lu, J. Yu, Y. Bai, W. Peng and R. Xu, *Langmuir*, 1999, **15**, 4837.
28 B. Li, Y. Bai, N. Lu, W. Pang and R. Xu, *Surf. Sci.*, 1999, **441**, 436.
29 H. Lin, H. Sakamoto, W. S. Seo, K. Kuwabara and K. Koumoto, *J. Cryst. Growth*, 1998, **192**, 250.
30 N. Kimizuka, T. Asai, S. Ohno, K. Fujiyoshi and T. Kunitake, *Surf. Sci.*, 1997, **386**, 245.
31 P. Calvert and P. Rieke, *Chem. Mater.*, 1996, **8**, 1715.
32 S. J. Cooper, R. B. Sessions and S. D. Lubetkin, *Langmuir*, 1997, **13**, 7165.
33 S. J. Cooper, R. B. Sessions and S. D. Lubetkin, *J. Am. Chem. Soc.*, 1998, **120**, 2090.
34 S. Champ, J. A. Dickinson, P. S. Fallon, B. R. Heywood and M. Mascal, *Angew. Chem., Int. Ed.*, 2000, **39**, 2716.
35 L. Lu, H. Cui, W. Li, H. Zhang and S. Xi, *Chem. Mater.*, 2001, **13**, 325.
36 P. J. J. A. Buijnsters, J. J. J. M. Donners, S. J. Hill, B. R. Heywood, R. J. M. Nolte, B. Zwanenburg and N. A. J. M. Sommerdijk, *Langmuir*, 2001, **17**, 3623.
37 E. V. Rakova, V. V. Klechkovskaya, N. D. Stepina and L. A. Feigin, *Crystallogr. Rep.*, 2002, **47**, S177.
38 L.-J. Zhang, H.-G. Liu, X.-S. Feng, R.-J. Zhang, L. Zhang, Y.-D. Mu, J.-C. Hao, D.-J. Qian and Y.-F. Lou, *Langmuir*, 2004, **20**, 2243.
39 M. J. Lochhead, S. R. Letellier and V. Vogel, *J. Phys. Chem. B*, 1997, **101**, 10821.
40 S. Whipps, S. R. Kahn, F. J. O'Palko, R. Backov and D. R. Talham, *J. Cryst. Growth*, 1998, **192**, 243.
41 S. R. Letellier, M. J. Lochhead, A. A. Campbell and V. Vogel, *Biochim. Biophys. Acta*, 1998, **1380**, 31.
42 S. Choudhury, N. Bagkar, G. K. Dey, H. Subramanian and J. V. Yakhmi, *Langmuir*, 2002, **18**, 7409.
43 J. X. He, S. Yamashita, W. Jones and A. Yamagishi, *Langmuir*, 2002, **18**, 1580.
44 L.-J. Zhang, H.-G. Liu, X.-S. Feng, D.-J. Qian, L. Zhang, X.-L. Yu and Q.-L. Feng, *Thin Solid Films*, 2004, **458**, 287.
45 J.-M. Ouyang, S.-P. Deng, J.-P. Zhong, B. Tieke and S.-H. Yu, *J. Cryst. Growth*, 2004, **270**, 646.

46 D. Volkmer, M. Fricke, D. Vollhardt and S. Siegel, *J. Chem. Soc., Dalton Trans.*, 2002, 4547.
47 D. Volkmer, M. Fricke, C. Agena and J. Mattay, *J. Mater. Chem.*, 2004, **14**, 2249.
48 D. Volkmer, M. Fricke, M. Gleiche and L. Chi, *Mater. Sci. Eng., C*, 2005, **25**, 161.
49 M. Fricke, D. Volkmer, C. E. Krill III, M. Kellerman and A. Hirsch, *Cryst. Growth Des.*, 2006, **6**, 1120.
50 R. Backov, C. M. Lee, S. R. Khan, C. Mingotaud, G. E. Fanucci and D. R. Talham, *Langmuir*, 2000, **16**, 6013.
51 J.-M. Ouyang and S.-P. Deng, *Colloids Surf., A*, 2005, **257-258**, 395.
52 D. R. Talham, R. Backov, I. O. Benítez, D. M. Sharbaugh, S. Whipps and S. R. Khan, *Langmuir*, 2006, **22**, 2450.
53 K. Sato, Y. Kumagai, K. Watari and J. Tanaka, *MRS Symp. Proc.*, 2004, EXS-1.
54 E. Loste, E. Díaz-Martí, A. Zarbakhsh and F. C. Meldrum, *Langmuir*, 2003, **19**, 2830.
55 I. O. Benítez and D. R. Talham, *Langmuir*, 2004, **20**, 8287.
56 D. M. Duffy and J. H. Harding, *Langmuir*, 2004, **20**, 7630.
57 S. Grayer Wolf, E. M. Landau, M. Lahav, L. Leiserowitz, M. Deutsch, K. Kjaer and J. Als-Nielsen, *Thin Solid Films*, 1988, **159**, 29.
58 D. Jacquemain, S. Grayer Wolf, F. Leveiller, M. Lahav, L. Leiserowitz, M. Deutsch, K. Kjaer and J. Als-Nielsen, *J. Am. Chem. Soc.*, 1990, **112**, 7724.
59 J. Majewski, R. Popovitz-Biro, K. Kjaer, J. Als-Nielsen, M. Lahav and L. Leiserowitz, *J. Phys. Chem.*, 1994, **98**, 4087.
60 B. Lin, T. M. Bohanon, M. C. Shih and P. Dutta, *Langmuir*, 1990, **6**, 1665.
61 M. C. Shih, T. M. Bohanon, J. M. Mikrut, P. Zschack and P. Dutta, *J. Chem. Phys.*, 1992, **96**, 1556.
62 C. Böhm, F. Leveiller, D. Jacquemain, H. Möwald, K. Kjaer, J. Als-Nielsen, I. Weissbuch and L. Leiserowitz, *Langmuir*, 1994, **10**, 830.
63 F. Leveiller, C. Böhm, D. Jacquemain, H. Möwald, L. Leiserowitz, K. Kjaer and J. Als-Nielsen, *Langmuir*, 1994, **10**, 819.
64 J. Kmetko, A. Datta, G. Evmenenko and P. Dutta, *J. Phys. Chem. B*, 2001, **105**, 10818.
65 J. Kmetko, A. Datta, G. Evmenenko, M. K. Durbin, A. G. Richter and P. Dutta, *Langmuir*, 2001, **17**, 4697.
66 S. Cantin, J. Pignat, F. Perrot, P. Fontaine and M. Goldmann, *Phys. Rev. E*, 2004, **70**, 50601.
67 J. Pignat, S. Cantin, R. C. W. Liu, M. Goldmann, P. Fontaine, J. Daillant and F. Perrot, *Eur. Phys. J. E*, 2006, **20**, 387.
68 E. DiMasi and L. B. Gower, *MRS Proc.*, 2001, **711**, 301.
69 E. DiMasi, M. J. Olszta, V. M. Patel and L. B. Gower, *CrystEngComm*, 2003, **5**, 346.
70 J. Kmetko, C. Yu, G. Evmenenko, S. Kewalramani and P. Dutta, *Phys. Rev. B*, 2003, **68**, 85415.
71 G. Xu, N. Yao, I. A. Aksay and J. T. Groves, *J. Am. Chem. Soc.*, 1998, **120**, 11977.
72 E. DiMasi, V. M. Patel, M. Sivakumar, M. J. Olszta, Y. P. Yang and L. B. Gower, *Langmuir*, 2002, **18**, 8902.
73 X. Xu, J. T. Han and K. Cho, *Chem. Mater.*, 2004, **16**, 1740.
74 J. Kmetko, C. Yu, G. Evmenenko, S. Kewalramani and P. Dutta, *Phys. Rev. Lett.*, 2002, **89**, 186102.
75 S. Kewalramani, G. Evmenenko, C.-J. Yu, K. Kim, J. Kmetko and P. Dutta, *Surf. Sci.*, 2005, **591**, L286.
76 S. Kewalramani, G. Dommett, K. Kim, G. Evmenenko, H. Mo, B. Stripe and P. Dutta, *J. Chem. Phys.*, 2006, **125**, 224713.
77 D. C. Popescu, M. M. J. Smulders, B. P. Pichon, N. Chebotareva, S.-Y. Kwak, O. L. J. van Asselen, R. P. Sijbesma, E. DiMasi and N. A. J. M. Sommerdijk, *J. Am. Chem. Soc.*, 2007, DOI: 10.1021/ja075875t.
78 Q. Huo, S. Russev, T. Hasegawa, J. Nishijo, J. Umemura, G. Puccetti, K. C. Russell and R. M. Leblanc, *J. Am. Chem. Soc.*, 2000, **122**, 7890.
79 T. Kobayashi and T. Seki, *Langmuir*, 2003, **19**, 9297.
80 M. R. J. Vos, G. E. Jardí, A. L. Pallas, M. Breurken, O. L. J. van Asselen, P. H. H. Bomans, P. E. L. G. Leclère, P. M. Frederik, R. J. M. Nolte and N. A. J. M. Sommerdijk, *J. Am. Chem. Soc.*, 2005, **127**, 16768.
81 J. Als-Nielsen, D. Jacquemain, K. Kjaer, F. Leveiller, M. Lahav and L. Leiserowitz, *Phys. Rep.*, 1994, **246**, 251.
82 V. M. Kaganer, H. Mohwald and P. Dutta, *Rev. Mod. Phys.*, 1999, **71**, 779.
83 H. Rapaport, I. Kuzmenko, M. Berfeld, K. Kjaer, J. Als-Nielsen, R. Popovitz-Biro, I. Weissbuch, M. Lahav and L. Leiserowitz, *J. Phys. Chem. B*, 2000, **104**, 1399.
84 Y. Politi, T. Arad, E. Klein, S. Weiner and L. Addadi, *Science*, 2004, **306**, 1161.
85 M. J. Olszta, D. J. Odom, E. P. Douglas and L. B. Gower, *Connect. Tissue Res.*, 2003, **44**, 326.
86 J. J. E. Moreau, B. P. Pichon, M. W. C. Man, C. Bied, H. Pritzkow, J.-L. Bantignies, P. Dieudonné and J.-L. Sauvajol, *Angew. Chem., Int. Ed.*, 2004, **43**, 203.
87 S. Cavalli, D. C. Popescu, E. E. Tellers, M. R. J. Vos, B. P. Pichon, M. Overhand, H. Rapaport, N. A. J. M. Sommerdijk and A. Kros, *Angew. Chem., Int. Ed.*, 2006, **45**, 739.

